MAREZIO, M., REMEIKA, J. P. & DERNIER, P. D. (1970*a*). *Acta Cryst.* B**26**, 300–302.
MAREZIO, M., REMEIKA, J. P. & DERNIER, P. D. (1970*b*). *Acta Cryst.* B**26**, 2008–2022.
MASLEN, E. N. & SPADACCINI, N. (1993). *Acta Cryst.* A**49**, 661–667.
MASLEN, E. N., STRELTSOV, V. A., STRELTSOVA, N. R. & ISHIZAWA, N. (1994). *Acta Cryst.* B**50**, 435–441.
MASLEN, E. N., STRELTSOV, V. A., STRELTSOVA, N. R. & ISHIZAWA, N. (1995). *Acta Cryst.* B**51**, AS682.
MASLEN, E. N., STRELTSOV, V. A., STRELTSOVA, N. R., ISHIZAWA, N. & SATOW, Y. (1993). *Acta Cryst.* B**49**, 973–980.
NATHANS, R., PICKART, S. J., ALPERIN, H. A. & BROWN P. J. (1964). *Phys. Rev. A*, **136**, 1641–1647.
O'KEEFFE, M. & HYDE, B. G. (1977). *Acta Cryst.* B**33**, 3802–3813.
O'KEEFFE, M. & HYDE, B. G. (1985). *An Alternative Approach to Non-Molecular Crystal Structures With Emphasis on the Arrangements of Cations. Structure and Bonding*, Vol. 61, pp. 77–144. Berlin: Springer-Verlag.
REES, B. (1977). *Isr. J. Chem.* **16**, 180–186.
REMEIKA, J. P. (1956). *J. Am. Chem. Soc.* **78**, 4259–4260.
REMEIKA, J. P. & KOMETANI, T. Y. (1968). *Mat. Res. Bull.* **3**, 895–900.
SATOW, Y. & IITAKA, Y. (1989). *Rev. Sci. Instrum.* **60**, 2390–2393.
TOFIELD, B. C. & FENDER, B. E. F. (1970). *J. Phys. Chem. Solids*, **31**, 2741–2749.
ZACHARIASEN, W. H. (1967). *Acta Cryst.* A**23**, 558–564.

Acta Cryst. (1995). B**51**, 929–939

Electron Density and Optical Anisotropy in Rhombohedral Carbonates. III.* Synchrotron X-ray Studies of $CaCO_3$, $MgCO_3$ and $MnCO_3$

BY E. N. MASLEN, V. A. STRELTSOV† AND N. R. STRELTSOVA

Crystallography Centre, University of Western Australia, Nedlands 6907, *Australia*

AND N. ISHIZAWA

Research Laboratory of Engineering Materials, Tokyo Institute of Technology, 4259 *Nagatsuta, Midori-Ku, Yokohama* 227, *Japan*

(*Received* 25 *November* 1994; *accepted* 15 *May* 1995)

Abstract

Diffraction-deformation electron-density ($\Delta\rho$) images for small, naturally faced single crystals of synthetic calcite ($CaCO_3$), magnesite ($MgCO_3$) and mineral rhodochrosite ($MnCO_3$) were measured with focused $\lambda = 0.7$ and 0.9 Å synchrotron (SR) X-radiation. Mo $K\alpha$ ($\lambda = 0.71073$ Å) structure factors were also measured for $MnCO_3$. Lattice mode frequencies predicted from eigenvalues of **T** and **L** tensors for CO_3 rigid-group motion in these structures are close to spectroscopic values. High approximate $\Delta\rho$ symmetry around the cations increases towards 6/*mmm* in the sequence $CaCO_3$, $MgCO_3$ to $MnCO_3$. The $\Delta\rho$ topography near the CO_3 groups shows the influence of the cations, and correlates strongly with the refractive indices, as required for a cause and effect relationship between electron density and optical anisotropy. Aspherical electron density around the Mn atom can be attributed to the effect of a non-ideal octahedral crystal field on the 3*d* electron distribution. The relationship of the $\Delta\rho$ topography near the Mn atom with that near the CO_3 group in $MnCO_3$ is consistent with magnetic interactions. Space group $R\bar{3}c$, hexagonal, $Z = 6$, $T = 295$ K: $CaCO_3$, $M_r = 100.09$, $a = 4.988\,(2)$, $c = 17.068\,(2)$ Å, $V = 367.8\,(3)$ Å^3, $D_x = 2.711$ Mg m^{-3}, $\mu_{0.7} = 1.93$ mm^{-1}, $F(000) = 300$, $R = 0.015$, $wR = 0.012$, $S = 3.0$ for 437 unique reflections; $MgCO_3$, $M_r = 84.31$, $a = 4.632\,(1)$, $c = 15.007\,(2)$ Å, $V = 278.8\,(2)$ Å^3, $D_x = 3.013$ Mg m^{-3}, $\mu_{0.9} = 0.99$ mm^{-1}, $F(000) = 252$, $R = 0.015$, $wR = 0.021$, $S = 4.34$ for 270 unique reflections; $MnCO_3$, $M_r = 114.95$, $a = 4.772\,(3)$, $c = 15.637\,(3)$ Å, $V = 308.4\,(4)$ Å^3, $D_x = 3.713$ Mg m^{-3}, $\mu_{0.7} = 5.62$ mm^{-1}, $F(000) = 330$, $R = 0.015$, $wR = 0.039$, $S = 3.38$ for 386 unique reflections of the SR data set and $a = 4.773\,(1)$, $c = 15.642\,(1)$ Å, $V = 308.6\,(1)$ Å^3, $D_x = 3.711$ Mg m^{-3}, μ(Mo $K\alpha$) = 5.86 mm^{-1}, $R = 0.017$, $wR = 0.024$, $S = 2.79$ for 368 unique Mo $K\alpha$ reflections.

Introduction

The birefringence of mineral carbonates, indicating the direction-dependent response of electrons to electric components of light waves, has been modelled repeatedly since the pioneering investigation (Bragg, 1924). We seek an atomic scale explanation for the optical anisotropy ($< n > /n$) of the rhombohedral carbonates listed in Table 1 that correlates with mean refractive index ($< n >$), but not with cell volume or *a*/*c* ratio. The refractive index n_e* for the electric vector along

* Parts I and II: Maslen, Streltsov & Streltsova (1993*a*,*b*).
† Author to whom correspondence should be addressed.

* The subscripts '*o*' and '*e*' denote, respectively, the ordinary and extraordinary components of light.

Table 1. *Optical and structural data for some rhombohedral carbonates (hexagonal unit cell)*

	a (Å)	c (Å)	a/c	$\bar{\rho}$ (e Å^{-3})	$\bar{\rho}$*	n_o	n_e	$\langle n \rangle$	$\Delta n/\langle n \rangle$	$\langle n \rangle^2 - 1$	$\langle n \rangle^2 - 1$*
$CaCO_3$[a]	4.988 (2)	17.068 (2)	0.292	0.816	1.000	1.6584	1.4864	1.601	0.107	1.564	1.000
$MgCO_3$[a]	4.632 (1)	15.007 (2)	0.309	0.904	1.108	1.700	1.509	1.636	0.117	1.676	1.072
$MnCO_3$[a]	4.772 (3)	15.637 (3)	0.305	1.070	1.311	1.816	1.597	1.743	0.126	2.038	1.303
$CdCO_3$[b]	4.923 (3)	16.287 (6)	0.302	1.369	1.678	1.85	1.60	1.767	0.142	2.121	1.357
$CoCO_3$[c]	4.6581	14.958	0.311	1.217	1.491	1.855	1.60	1.770	0.144	2.133	1.364
$ZnCO_3$[d]	4.6526 (7)	15.026 (2)	0.310	1.278	1.566	1.848	1.621	1.772	0.128	2.141	1.369
$FeCO_3$[d]	4.6916 (4)	15.380 (2)	0.305	1.146	1.404	1.875	1.633	1.794	0.135	2.220	1.419
$NiCO_3$[c]	4.5975	14.723	0.312	1.291	1.582	1.913	1.692	1.839	0.120	2.383	1.524

Unit-cell parameters are from: (*a*) present synchrotron data; (*b*) Borodin, Lyutin, Ilyukhin & Belov (1979); (*c*) Graf (1961); (*d*) Effenberger, Mereiter & Zemann (1981).

Refractive indices n_o and n_e for the sodium D line ($\lambda = 5890$ A) are from Isherwood & James (1976).

$\langle n \rangle = 1/3(2n_o + n_e)$ – the mean refractive index.

$\bar{\rho} = N/V$ – the mean of the total electron density.

* Relative to $CaCO_3$ values.

the unique hexagonal c axis is markedly smaller than n_o, with the electric vector normal to c.

At visible light frequencies, n depends only on electron polarization and thus on how the electrons bind to the nuclear framework. If the reradiation characteristics of that framework are anisotropic, the refractive index changes with direction. Explanation thus reduces to ascertaining which of structural distortion, electron redistribution or other factors are primarily responsible for the optical anisotropy.

The mineral carbonates are covalent insulators. Covalent bonding is often typified by electron-density accumulation between atoms. Such accumulation of loosely bound electrons contributes strongly to crystal polarizability and electric susceptibility, because potential gradients in bonding regions are lower than those in non-bonding directions.

What is true for chemical bonds may also apply to lone pairs. Whereas tightly bound electrons screening nuclei contribute little to susceptibility, mobile weakly bound electrons are largely responsible for covalent insulators' high susceptibilities. Their ϵ_2-spectra (ϵ_2 being the imaginary part of the complex dielectric constant) confirm that core-electron excitation is relatively less important than valence-electron excitation for some ferroelectric oxides (Mamedov, Shilnikov, Mehdiev & Ibragimova, 1984) compared with simpler oxides (*e.g.* Hanson, Arakawa & Williams, 1972). A crystal's main contribution to refractive index comes from low potential regions with high electron density. Accurate diffraction imaging of that electron density could provide insight into the components of a crystal's electron density that are mainly responsible for optical anisotropy. Properties dependent ultimately on local polarization could thus be explored by measuring electron density.

We first study possible correlations between the dielectric function (or refractive indices) and electron densities in crystals by considering harmonic oscillator models that should prove adequate for insulators containing covalently bonded CO_3 moieties, since bond and lone-pair electrons are bound more or less tightly to atoms. Such models may be less adequate for strongly ionic crystals with large and asymmetric bonding potentials.

The mean electron density $\bar{\rho} = N/V$ for the N charged oscillators in a crystal is excited by electromagnetic radiation. Strong correlation of that mean density with refractive index n is expected from the equation relating refractive index to oscillator strength (Kittel, 1986)

$$n^2 - 1 = (e^2\bar{\rho})/\epsilon_0 K, \qquad (1)$$

where e is the electron charge. For rigid electron density the restoring force constant K due to the atomic potentials would determine the oscillator eigenfrequency. Expression (1) holds for cubic crystals, even if some atom sites do not have high symmetry. For uniaxial crystals such as carbonates, expression (1) remains true on replacing n by $< n >= \frac{1}{3}(2n_o + N_e)$. In general, due to crystal anisotropy, polarization and field strength are not in the same direction.

The $< n >^2 - 1$ ratios for $CaCO_3$, $MgCO_3$ and $MnCO_3$ correlate strongly with the mean unit-cell electron density ($\bar{\rho}$) (Table 1), but vary more slowly than for some other carbonates, because inner electron polarizabilities are lower for atoms with high atomic number.

Weber (1988) related optical properties of crystals to bond orientation and polarizibility, showing that anisotropic bond polarizabilities were mainly responsible for optical anisotropy in MCO_3 and MSO_4 (M = Mg, Ca, Sr, Ba). Anion groups are the main cause of the birefringence. Whereas C—O and S—O bond anisotropies in other crystals are often similar, additional parameters were required to describe local fields in such compounds, indicating structure-dependent variation of CO_3 and SO_4 group polarizabilities.

Tossel & Lazzeretti (1988) calculated frequency-dependent electric dipole polarizability tensors for isolated CO_3^{2-} and Ca^{2+} components in $CaCO_3$ using large Gaussian basis-set *ab initio* random-phase approximations. Refractive index estimates using $\sim$1.3 times the isotropic polarizability calculated for a Ca^{2+} ion agreed with experiment. All available results

confirm that anisotropic polarizability of the CO_3 group electron density is the main cause of birefringence in rhombohedral carbonates – an inference consistent with the anisotropic carbonate group geometry.

Our immediate aim in this investigation was to study the redistribution of bonding electron density ($\Delta\rho$) for the CO_3 groups in these isostructural crystals. *Ab initio* all-electron periodic Hartree–Fock calculations for $MgCO_3$ and $CaCO_3$ were performed using the *CRYSTAL* program by Catti, Pavese, Dovesi & Saunders (1993) and Catti, Pavese, Apra & Roetti (1993), respectively. The general topography of all theoretical $\Delta\rho$ maps resembles those evaluated from diffraction data by Maslen, Streltsov & Streltsova (1993*a*,*b*), although the experimental $CaCO_3$ $\Delta\rho$ is more diffuse and depleted than that for $MgCO_3$. The static theoretical $\Delta\rho$ in the CO_3 group plane for $CaCO_3$ closely resembles the corresponding experimental $MgCO_3$ map.

Following earlier Mo $K\alpha$ measurements using synthetic calcite and mineral magnesite, the weaker structure factors for synthetic $MgCO_3$ and new specimens of synthetic $CaCO_3$ are now remeasured more precisely with synchrotron X-radiation. To study the influence of metal 3*d* electrons, structure factors for a mineral sample of $MnCO_3$ were measured both with Mo $K\alpha$ and with synchrotron radiation. Although essentially antiferromagnetic, crystalline $MnCO_3$ is weakly ferromagnetic. There have been several experimental and theoretical studies of such small spontaneous magnetization, first observed in haematite, α-Fe_2O_3. The magnetic and chemical cells in $MnCO_3$ are identical, with electron spins in the basal plane. The weak ferromagnetism in the basal plane agrees with the Dzialoshinskii (1957) theory of antisymmetric superexchange that causes spin canting.

Polarized neutron studies of the ferromagnetic moment distribution in $MnCO_3$ by Brown & Forsyth (1967) and in α-Fe_2O_3 by Nathans, Pickart, Alperin & Brown (1964) showed moment distributions around magnetic cations that deviate markedly from spherical symmetry. Spin density was located both near to and far from the magnetic atoms, particularly near the CO_3 group in $MnCO_3$. Projected ferromagnetic spin densities around the Mn atoms within the MnO_6 octahedra extend to nearby O atoms, indicating that the weak ferromagnetism is more complicated than simple canting of magnetic moments. Analysis of polarized neutron-diffraction data for $MnCO_3$ by Lindgård & Marshall (1969) showed that covalency between the Mn cation and six neighbouring O atoms, along with exchange polarization in the CO_3 anion, can account for the main spin-density features in $MnCO_3$.

Accurate diffraction imaging of electron density in compounds with cation structural geometry approximating symmetry higher than the lattice symmetry improves our understanding of basic interactions in solids. Approximate sixfold electron-density symmetry near Al and Fe cations, respectively, for α-Al_2O_3 (Maslen, Streltsov, Streltsova, Ishizawa & Satow, 1993) and α-Fe_2O_3 (Maslen, Streltsov, Streltsova & Ishizawa, 1994) is higher than the threefold symmetry expected for cation–oxygen bonding, indicating that cation–cation interactions make a stronger than expected impact on the electron density.

The CO_3 group, having covalent bonds with relatively high force constants, behaves as a rigid segment in carbonate minerals. Their vibrational spectra separate into internal and lattice modes to a good approximation. The CO_3 group rigid-body vibrations generate low-frequency lattice translation and libration modes active in the far-IR and Raman spectra (White, 1974). Finger (1975) demonstrates how well rigid-body motions determined from diffraction experiments convert into lattice motions that correlate with spectroscopic data for calcite and magnesite, resolving ambiguities in spectral assignments and allowing frequencies to be determined for IR-inactive vibrations. Vibration frequencies evaluated from synchrotron diffraction data for $CaCO_3$, $MgCO_3$ and $MnCO_3$ provide independent checks on parameters that minimize differences between observed and calculated structure factors.

Experimental

A $MgCO_3$ crystal synthesized hydrothermally following Oh, Morikawa, Iwai & Aoki (1973), a $CaCO_3$ specimen from aqueous solution grown as described by Maslen, Streltsov & Streltsova (1993*a*) and a cleavage fragment of mineral $MnCO_3$ from the Mineralogical Museum of the University of Western Australia were each bounded by two (104), two ($\bar{1}$14) and two (0$\bar{1}$4) faces. Crystal-face indices and dimensions 9 × 9 × 8, 12 × 14 × 11 and 40 × 24 × 49 μm^3, respectively, from the centre were determined using optical and scanning electron Philips SEM505 microscopes. Electron-beam-induced X-ray microanalysis of the rhodochrosite sample with an energy-dispersive spectrometer indicated negligible Mg, Ca and Fe impurities.

Following previous studies of $CaCO_3$ and $MgCO_3$ by Maslen, Streltsov & Streltsova (1993*a*,*b*), preliminary structure factors for $MnCO_3$ were measured on a Syntex P3 four-circle diffractometer using Mo $K\alpha$ (λ = 0.71073 Å) radiation from an X-ray tube monochromated by an equatorial setting oriented graphite crystal. Diffraction intensity data for $CaCO_3$ and $MnCO_3$ were measured with 0.7000 (2) Å wavelength synchrotron X-radiation on BL14A at the Tsukuba Photon Factory. Counting statistics for the smaller $MgCO_3$ crystal were improved by changing the synchrotron beam wavelength to 0.9000 (2) Å, increasing the incident synchrotron beam flux by a factor of almost ten.

The vertically polarized radiation from the BL14A wiggler was monochromated by a double Si (111) crystal monochromator, using a curved mirror to focus the X-rays onto the four-circle diffractometer (Satow &

Table 2. *Experimental details*

Crystal data				
Chemical formula	$MnCO_3$	$MnCO_3$	$CaCO_3$	$MgCO_3$
Chemical formula weight	114.95	114.95	100.09	84.31
Cell setting	Trigonal	Trigonal	Trigonal	Trigonal
Space group	$R\bar{3}c$	$R\bar{3}c$	$R\bar{3}c$	$R\bar{3}c$
a (Å)	4.773 (1)	4.772 (3)	4.988 (2)	4.632 (1)
b (Å)	4.773 (1)	4.772 (3)	4.988 (2)	4.632 (1)
c (Å)	15.642 (1)	15.637 (3)	17.068 (2)	15.007 (2)
α (°)	90.0	90.0	90.0	90.0
β (°)	90.0	90.0	90.0	90.0
γ (°)	120.0	120.0	120.0	120.0
V (Å^3)	308.6 (1)	308.4 (4)	367.8 (3)	278.8 (2)
Z	6	6	6	6
D_x ($Mg\ m^{-3}$)	3.711	3.713	2.711	3.013
Radiation type	Mo $K\alpha$	Synchrotron	Synchrotron	Synchrotron
Wavelength (Å)	0.71073	0.7000 (2)	0.7000 (2)	0.9000 (2)
No. of reflections for cell parameters	33	6	6	12
θ range (°)	11.15–44.10	88.99	83.90	55.37–99.52
μ (mm^{-1})	5.86	5.62	1.93	0.99
Temperature (K)	295	295	295	295
Data collection				
Diffractometer	Syntex P3	BL14A four-circle	BL14A four-circle	BL14A four-circle
Data collection method	ω–2θ	ω–2θ	ω–2θ	ω–2θ
Absorption correction	Analytical	Analytical	Analytical	Analytical
T_{min}	0.568	0.580	0.900	0.942
T_{max}	0.779	0.788	0.936	0.988
No. of measured reflections	3910	4096	4793	2701
No. of independent reflections	368	386	437	270
R_{int}	0.065	0.095	0.26	0.027
θ_{max} (°)	100	100	100	130
Range of h, k, l	$-10 \rightarrow h \rightarrow 10$ $-10 \rightarrow k \rightarrow 10$ $-33 \rightarrow l \rightarrow 33$	$-10 \rightarrow h \rightarrow 10$ $-10 \rightarrow k \rightarrow 10$ $-34 \rightarrow l \rightarrow 34$	$-10 \rightarrow h \rightarrow 10$ $-10 \rightarrow k \rightarrow 10$ $-36 \rightarrow l \rightarrow 36$	$-9 \rightarrow h \rightarrow 9$ $-9 \rightarrow k \rightarrow 9$ $-30 \rightarrow l \rightarrow 30$
No. of standard reflections	6	6	6	6
Frequency of standard reflections	100	100	100	100
Intensity decay (%)	9.7	2.8	4.2	9.7
Refinement				
Refinement on	F	F	F	F
R	0.017	0.015	0.015	0.015
wR	0.024	0.039	0.012	0.021
S	2.79	3.38	3.0	4.34
No. of reflections used in refinement	368	386	437	270
No. of parameters used	10	10	10	10
Weighting scheme	$w = 1/\sigma^2(F)$	$w = 1/\sigma^2(F)$	$w = 1/\sigma^2(F)$	$w = 1/\sigma^2(F)$
$(\Delta/\sigma)_{max}$	0.1×10^{-3}	0.2×10^{-4}	0.1×10^{-3}	0.2×10^{-3}
$\Delta\rho_{max}$ (e Å^{-3})	0.74	0.89	0.44	0.56
$\Delta\rho_{min}$ (e Å^{-3})	−0.45	−1.49	−0.49	−0.48
Extinction method	Maslen & Spadaccini (1993)	Maslen & Spadaccini (1993)	Maslen & Spadaccini (1993)	Maslen & Spadaccini (1993)
Extinction coefficient	Negligible	Negligible	0.11 (5) $\times 10^4$	Negligible
$\sigma(\Delta\rho)$* (e Å^{-3})	0.05	0.15	0.06	0.04
Extinction method	Least-squares (Zachariasen, 1967)	Least-squares (Zachariasen, 1967)	Least-squares (Zachariasen, 1967)	Least-squares (Zachariasen, 1967)
Extinction coefficient	Negative	Negative	0.11 (5) $\times 10^4$	Negative
Source of atomic scattering factors	*International Tables for X-ray Crystallography* (1974, Vol. IV)			

* Mean e.s.d. value (Cruickshank, 1949).

Iitaka, 1989). The polarization ratio, *i.e.* the fraction of the total incident beam intensity with its electric vector vertical, was 0.95. As the positron beam decays exponentially with time, the incident beam intensity was monitored with an ion chamber. An incident beam slit was installed before the monitor ion counter. A pinhole slit 0.4 mm wide provided an intense and adequately homogeneous beam. Positioning the specimen slightly off-focus minimized the changes in the synchrotron radiation intensity due to particle beam instabilities. The first monochromator crystal alignment and vertical translations for the mirror were automatically optimized every 20 min by flux maximization during data collection, holding the incident beam stable to within 1% over 1 d. A 3 × 3 mm receiving slit was placed in front of the scintillation counter. Further details are given in Table 2.

Lattice constants were determined from 12 reflections with 2θ values ($55.37 < 2\theta < 99.52°$) for $MgCO_3$, six equivalent reflections at 2θ values of 83.90° for $CaCO_3$ and 88.99° for the $MnCO_3$ SR data, and from 33 reflections with 2θ values ($11.15 < 2\theta < 44.10°$) for the $MnCO_3$ Mo $K\alpha$ data. Reflection intensities were measured systematically using $\omega/2\theta$ scans for the complete sphere of reciprocal space with $(\sin\theta/\lambda)_{max}$ = 1.006 Å^{-1}, $-9 \le h \le 9$, $-9 \le k \le 9$, $-30 \le l \le 30$ for $MgCO_3$, $(\sin\theta/\lambda)_{max}$ = 1.094 Å^{-1}, $-10 \le h \le 10$, $-10 \le k \le 10$, $-36 \le l \le 36$ for $CaCO_3$ and $-10 \le h \le 10$, $-10 \le k \le 10$, $-34 \le l \le 34$ for the $MnCO_3$ SR data set and with $(\sin\theta/\lambda)_{max}$ = 1.078 Å^{-1}, $-10 \le h \le 10$, $-10 \le k \le 10$, $-33 \le l \le 33$ for the $MnCO_3$ Mo $K\alpha$ data. Six standard reflections were measured every 100 reflections to monitor the incident beam stability. Integrated intensities for all the accessible reflections measured for $MnCO_3$ with Mo $K\alpha$ radiation were calculated using the profile analysis program by Streltsov & Zavodnik (1989), allowing the weaker beams diffracted from the small crystal to be evaluated more accurately. The measured intensities were modified for fluctuation of the standards and the variances adjusted as suggested by Rees (1977). Variances in the measured structure factors evaluated from counting statistics were modified for source instability, as indicated by the standards. Reflections having measured variances consistent with Poisson statistics were assigned that variance. Variances for the other reflections were increased where necessary according to the scatter of equivalents following a Fisher test. No reflections were classified arbitrarily as 'unobserved'.

Lorentz and polarization were applied. Absorption corrections (Alcock, 1974) were evaluated analytically. The reference state for structure-factor calculations was the independent atom model (IAM) evaluated using spherical atomic scattering factors from *International Tables for X-ray Crystallography* (1974, Vol. IV), with dispersion corrections $\Delta f'$, $\Delta f''$ of 0.074, 0.060 for Mg, 0.009, 0.005 for C, 0.018, 0.010 for O at 0.9 Å, 0.223, 0.299 for Ca, 0.332, 0.712 for Mn, 0.007, 0.002 for C, 0.011, 0.006 for O at 0.7 Å, 0.336, 0.732 for Mn, 0.007, 0.002 for C, and 0.012, 0.006 for O at Mo $K\alpha$, evaluated by Creagh (1992). All subsequent calculations utilized the *Xtal*3.2 system of crystallographic programs (Hall, Flack & Stewart, 1992) implemented on Sun Sparc and DEC 5000/120 workstations.

Ten independent structural parameters, including anisotropic vibration tensor elements, were determined by full-matrix least-squares refinement residuals based on $|F|$ weighted by $1/\sigma^2(F_o)$ for all measured structure factors. Details are included in Tables 2 and 3.*

Table 3. *Fractional coordinates x, anisotropic vibration parameters U_{ij} (Å^2), some interatomic distances (Å) and rigid-body vibration parameters for* $CaCO_3$, $MgCO_3$ *and* $MnCO_3$

		$CaCO_3$ SR	$MgCO_3$ SR	$MnCO_3$ Mo $K\alpha$	$MnCO_3$ SR
6Me on 6(*b*)	U_{11}	0.00988 (3)	0.00623 (9)	0.00777 (6)	0.00944 (9)
(0, 0, 0)	U_{33}	0.00932 (4)	0.0075 (1)	0.00966 (9)	0.01125 (8)
6C on 6(*a*)	U_{11}	0.00834 (9)	0.0056 (2)	0.0064 (2)	0.0081 (4)
(0, 0, ¼)	U_{33}	0.0108 (2)	0.0059 (2)	0.0074 (4)	0.0099 (3)
18O on 18(*e*)	x	0.25700 (6)	0.27748 (7)	0.2695 (1)	0.26975 (8)
(x, 0, ¼)	U_{11}	0.01129 (7)	0.00548 (9)	0.0068 (2)	0.0085 (1)
	U_{22}	0.0220 (2)	0.0077 (1)	0.0103 (2)	0.0117 (1)
	U_{33}	0.0202 (1)	0.0096 (1)	0.0123 (3)	0.0148 (1)
	U_{13}	−0.00424 (6)	−0.00057 (5)	−0.0009 (1)	−0.00099 (5)
C—O		1.2820 (5)	1.2852 (3)	1.2861 (7)	1.2873 (8)
		1.2880 (6)*	1.2860 (3)*	1.2880 (7)*	1.2890 (7)*
Me—O^{i}		2.3593 (7)	2.1009 (3)	2.1928 (7)	2.1916 (9)
O—O^{ii}		2.2206 (8)	2.2260 (4)	2.2275 (9)	2.230 (1)
O—O^{i}		3.1892 (4)	2.8474 (4)	2.9546 (5)	2.9539 (6)
O—O^{iii}		3.260 (2)	2.9239 (5)	3.0542 (9)	3.052 (2)
O—O^{iv}		3.4111 (6)	3.0175 (4)	3.1474 (5)	3.1460 (7)
CO_3†	T_{11} (Å^2)	0.006 (6)	0.004 (2)	0.005 (3)	0.007 (3)
	T_{33} (Å^2)	0.015 (2)	0.0081 (5)	0.0103 (7)	0.0125 (7)
	L_{11} (rad^2)	0.001 (2)	0.0004 (6)	0.0005 (7)	0.0005 (8)
	L_{33} (rad^2)	0.009 (2)	0.0016 (5)	0.0026 (7)	0.0024 (8)
	S_{11} (rad^2)	0.002 (1)	0.0003 (4)	0.0005 (5)	0.0005 (5)

Symmetry codes: (i) $\frac{2}{3} - x, \frac{1}{3} - y, \frac{1}{3} - z$; (ii) $-y, x - y, z$; (iii) $1 - y, x - y, z$; (iv) $\frac{2}{3} + y, \frac{1}{3} - x + y, \frac{1}{3} - z$.

* The C—O distance corrected for riding motion.

† Centre which gives symmetric S tensor: −0.004, −0.001, 0.140 for $CaCO_3$; 0.0, −0.003, 0.159 for $MgCO_3$; 0.0, −0.001, 0.158 for $MnCO_3$.

Before the structural parameters were refined, all $|F_o|$ values were corrected for secondary extinction by analysing equivalent reflections (Maslen & Spadaccini, 1993). That procedure yielded satisfactory extinction corrections in previous studies on small crystals of carbonate compounds (Maslen, Streltsov & Streltsova, 1993*a*,*b*). The largest correction (y_{min} = 0.95) for $CaCO_3$ approximated the value which optimized the extinction parameter r^* as part of the least-squares structure refinement (Larson, 1970). For $MgCO_3$ and $MnCO_3$ no significant extinction was indicated by comparison of equivalents, although significantly negative r^* parameters were indicated by least-squares structure refinements in both cases. Maslen, Streltsov & Streltsova (1993*b*) report similar results for their earlier refinement of $MgCO_3$. The least-squares residuals for both the rhodochrosite and magnesite refinements were dominated by particular low-angle reflections, for which $|F_o|$ exceeds the $|F_c|$ values predicted by the IAM. The $|F_o - F_c|$ discrepancies range up to 54σ (SR data) and 37σ (Mo $K\alpha$ data) for the 006 reflection of $MnCO_3$. To reduce these residuals the least-squares process indicated significant but non-physical negative extinction parameters and correspondingly biased scale factors. More reasonable scale factors for $MgCO_3$ and $MnCO_3$ data sets were determined in a final stage of refinement assigning equal weights to all reflections.

* Lists of structure factors and sections of $\Delta\rho$ for $MnCO_3$ Mo $K\alpha$ data have been deposited with the IUCr (Reference: AS0682). Copies may be obtained through The Managing Editor, International Union of Crystallography, 5 Abbey Square, Chester CH1 2HU, England.

Structural distortion

The structural geometry for these rhombohedral carbonates is fully described in earlier literature and by Maslen, Streltsov & Streltsova (1993*a*,*b*). The O-atom distribution approximates hexagonal close packing. Cations occupy trigonally distorted octahedral interstices. The metal-atom coordination is illustrated in Fig. 1. Each cation is surrounded by six O atoms at the vertices of an octahedron. Neither the *M*—O nor the O—O distances listed in Table 3, with the corresponding values for other carbonates (Effenberger, Mereiter & Zemann, 1981) correlate simply to their refractive indices.

Maslen, Streltsov & Streltsova (1993*a*,*b*) erroneously reported that the MO_6 octahedron is flattened in the *c* direction. The octahedron distortion ratio $O—O^{iv}/O—O^{iii}$ for $CaCO_3$, $MgCO_3$ and $MnCO_3$ is 1.0464 (6), 1.0321 (2) and 1.0308 (7), based on distances for the SR data from Table 3. As the $O—O^{iii}$ vector is normal to *c*, whereas $O—O^{iv}$ has a large component parallel to the threefold axis, the octahedron is elongated along *c*. The octahedron has the form of a trigonal antiprism with $\bar{3}2/m$ symmetry. The octahedral edge lengths in Table 3 indicate that the faces of the MO_6 octahedron for calcite are significantly larger than those in magnesite and rhodochrosite. The larger faces, especially in the basal plane, facilitate interactions between the cation and nearby atoms that may affect the electron-density distribution and vibrational motion. It is perhaps surprising that these octahedron distortion ratios correlate inversely with the refractive indices listed above.

The refractive indices also correlate inversely with the $O—O^{i}/O—O^{iii}$ ratio, of 0.9783 (6), 0.9738 (2) and 0.9679 (7) for $CaCO_3$, $MgCO_3$ and $MnCO_3$, respectively, and *a fortiori* with the ratio $[(O—O^{i})(O—O^{iv})]^{1/2}/(O—O^{iii})$, of 1.0117 (6), 1.0025 (2) and 0.998 (7) for $CaCO_3$, $MgCO_3$ and $MnCO_3$, which provides a stringent test of uniform progression through the series.

Notwithstanding this strong correlation of the coordination octahedron distortion with refractive indices, it cannot be a cause and effect relationship, as the correlation behaviour changes for other carbonate series compounds with higher refractive indices. For example, refractive indices for $ZnCO_3$ and $FeCO_3$ (Table 1) do not correlate inversely with distortion of the octahedral coordination, indicated by ratios $[(O—O^{i})(O—O^{iv})]^{1/2}/(O—O^{iii})$ of 0.9983 (6) and 1.0060 (6) for crystalline $ZnCO_3$ and $FeCO_3$ determined from the structural studies by Effenberger, Mereiter & Zemann (1981). This indicates the importance of electronic configuration, and not cation size alone. The low degree of correlation between refractive index and interatom distances indicates that these indices are insensitive to first-order changes in structural geometry. It would be unreasonable to argue that the refractive index variations result from changes in contact distance ratios that depend only at second order on interatom distances.

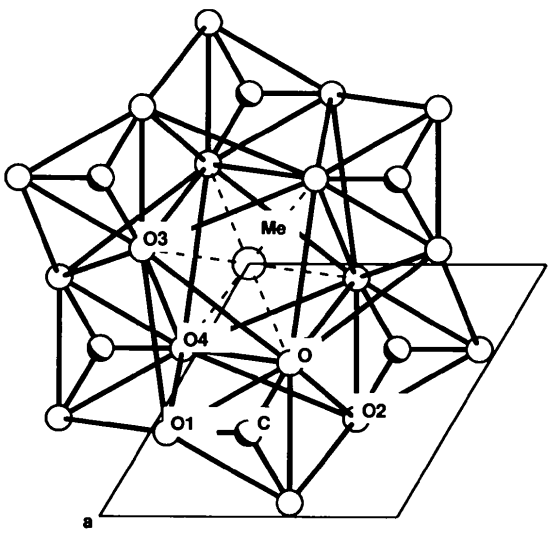

Fig. 1. Projection down the hexagonal *c* axis of a portion of the calcite structure showing the central cation coordinated to six O atoms from different CO_3 groups.

Atomic vibrations

Calcite, rhodochrosite and magnesite have increasingly compact unit cells. That ordering, so evident in both the *M*—O bond lengths and O—O distances, is also reflected in the C- and O-atom vibrational parameters (Table 3) being largest for $CaCO_3$ and smallest for $MgCO_3$. This is especially pronounced for the O atoms which for calcite have U_{ij} values more than 1.5 times those for the other carbonates in Table 3, suggesting that the electron density near the O-atom sites in calcite is smeared out considerably. As proposed by Reeder (1983) in relation to the *M*—C interactions through the basal octahedral face, the O atoms may play a significant role in 'shielding' the metal cations, explaining the larger vibration parameters in calcite for which the basal face is large.

Rigid-body motions for a CO_3 group with site symmetry 32 may be represented by five independent coefficients (Schomaker & Trueblood, 1968), two each for the translation **T** and libration **L** and one for the coupling tensor **S**. Tensor elements evaluated from the U_{ij} tensors for the C and O atoms compiled in Table 3 are close to those determined by Finger (1975) for mineral magnesite and calcite. There are significant translations along and librations about the threefold axis in all carbonates. The CO_3 group libration about the threefold axis has an appreciable screw component. Following Finger (1975) lattice-mode vibration frequencies for these carbonate structures were predicted from the **T** and **L** tensor eigenvalues. The mean-square rotational

motion amplitudes for **L** relate to harmonic oscillator frequencies ω by the expression (Prince, Schroeder & Rush, 1973)

$$A^2 = [h/(8\pi^2\omega cI)]\coth[(hc\omega)/2kT], \qquad (2)$$

where A^2 is the mean-square amplitude in radians, I is the group moment of inertia, and the other quantities have their usual meanings. The equation extends to translations by substituting the mean-square amplitude of linear motion for A^2 and the mass of the molecule or functional group for the moment of inertia I.

The IR frequencies inferred are compared with calculated values in Table 4. The $CaCO_3$ and $MgCO_3$ values agree with those by Finger (1975). All libration frequencies about the threefold axis of the CO_3 group from the present study are close to spectroscopic measurements. Those for the other librations and translations agree less well with spectroscopic data. It is possible that the modes with frequencies ν_9 and ν_{10}, having the same E_u symmetry, cannot be distinguished accurately in IR spectra (Finger, 1975). The ν_{11} mode should be active in inelastic neutron scattering.

The U_{11} vibration amplitudes for the metal atoms follow the trend that is evident for the CO_3 groups, but the Mn-atom vibrations parallel to c, reflected in the U_{33} values, are stronger than might have been predicted from the CO_3 group amplitudes. In no case does the trend for the vibrations correlate strongly with the refractive indices.

Table 4. *Vibrational frequencies* (cm^{-1}) *for* $CaCO_3$, $MgCO_3$ *and* $MnCO_3$

Mode*	Vibration parameter	Frequencies ν_t†	Frequencies ν_l†	Frequencies ν‡	Finger (1975)	Present work (SR data)
$CaCO_3$						
ν_7	L_{33}	92	136	106	104 (2)	103 (12)
ν_9	L_{11}	223	239	229	186 (7)	145 (154)
ν_{10}	T_{11}	102	123	106	119 (2)	149 (119)
ν_{11}§	T_{33}	—	—	—	107 (3)	87 (5)
$MgCO_3$						
ν_7	L_{33}	230	281	231	240 (22)	246 (46)
ν_9	L_{11}	301	315	263	387 (10)	223 (193)
ν_{10}	T_{11}	225	241	158	163 (5)	166 (39)
ν_{11}§	T_{33}	—	—	—	131 (6)	121 (4)
$MnCO_3$						
ν_7	L_{33}	—	—	181	—	197 (37)
ν_9	L_{11}	—	—	198	—	191 (170)
ν_{10}	T_{11}	—	—	157	—	134 (31)
ν_{11}§	T_{33}	—	—	—	—	97 (3)

* Mode notation from White (1974).

† ν_t and ν_l from IR reflectance spectra for single crystals by Hellwege, Lesch, Plihal & Schaack (1970).

‡ Lattice modes for powder samples from Morandat, Lorenzelli & LeComte (1967).

§ This mode is inactive in both IR and Raman spectra.

Table 5. *Atomic charges in electrons from the Hirshfeld partitioning of* $\Delta\rho$ *for* $CaCO_3$, $MgCO_3$ *and* $MnCO_3$

	$CaCO_3$	$MgCO_3$	$MnCO_3$	
	SR	SR	Mo $K\alpha$	SR
Me	+0.32 (3)	+0.28 (1)	+0.86 (5)	+0.48 (9)
C	+0.40 (3)	+0.26 (1)	+0.34 (4)	+0.30 (8)
O	−0.24 (2)	−0.18 (1)	−0.40 (3)	−0.26 (6)

Atomic charges

Atomic charges determined by projecting $\Delta\rho$ onto atomic density basis functions (Hirshfeld, 1977) are listed in Table 5. The interatom charge transfers are consistent in sign with expectations from atomic electronegativities, but their magnitudes are small. The SR charges listed in Table 5 are close to three Mo $K\alpha$ data values determined by Maslen, Streltsov & Streltsova (1993*a*) for $CaCO_3$. However, the SR charges for $MgCO_3$ and $MnCO_3$ agree less well with those determined by Maslen, Streltsov & Streltsova (1993*b*) and those derived from Mo $K\alpha$ data included in Table 4, particularly for the cations. It should be noted that the atomic charges presented by Maslen, Streltsov & Streltsova (1993*a*,*b*) are too low by a factor of 2. The charges were inadvertently calculated for one half of the formula unit. Throughout all the analyses the C-atom charges are relatively stable compared with the cation and oxygen charges. It is perhaps not surprising that the main effect of the cations on the integrated electron density for the CO_3 group atom relates to the O atoms that coordinate with the cation in the structure. Within the error in their determination the interatom charge-transfer values do not correlate significantly with other physical properties for these structures.

Electron density

The $< n >^2 - 1$ ratios for $CaCO_3$, $MgCO_3$ and $MnCO_3$ correlate strongly with the mean electron densities, as seen from Table 1, a result consistent with a cause and effect relationship between electron density and refractive index.

In order to test that possibility, the topography of $\Delta\rho$ maps for the (0001) plane through the CO_3 group and the (01$\bar{1}$0) plane through the M, C and O atoms shown in Figs. 2, 3 and 4 (SR data), for $CaCO_3$, $MgCO_3$ and $MnCO_3$, respectively, was studied carefully. The $CaCO_3$ maps are based on extinction corrections determined from equivalent reflection intensities by the method of Maslen & Spadaccini (1993). The 0.1 e Å^{-3} contour interval in Figs. 2 and 3 is approximately twice the $\sigma(\Delta\rho)$ values listed in Table 2 for $CaCO_3$ and $MgCO_3$. The $\sigma(\Delta\rho)$ value for $MnCO_3$ is somewhat larger. The complexity of the $\Delta\rho$ topography near the metal nucleus increases with atomic number in the sequence Mg, Ca and Mn, as expected on chemical grounds. The degree of local symmetry in the density around the cations, being higher than the site symmetry, encourages confidence in the physical significance of the $\Delta\rho$ maps.

Noise is far more pronounced in equivalent sections for $MnCO_3$ evaluated with Mo $K\alpha$ data and deposited

with the supplementary material* than in those for synchrotron data shown in Fig. 4, as also occurred in earlier $\Delta\rho$ maps evaluated with X-ray tube data. Allowing for the increased noise, the deposited maps are consistent with Figs. 4(*a*) and (*b*). That is the expected consequence of poor counting statistics for the predominantly weak reflections from small crystals measured with low-intensity X-ray sources.

The $\Delta\rho$ topography near the CO_3 group progresses uniformly from calcite, through magnesite to rhodochrosite. Density maxima in the C—O bonds are 0.43 e Å^{-3} high and those at the O-atom lone pairs are 0.15 e Å^{-3} high (Fig. 2). Corresponding C—O bond values for $MgCO_3$ and $MnCO_3$ are 0.56 and 0.64 e Å^{-3}, respectively. The O-atom lone-pair values are 0.25 and 0.40 e Å^{-3} (Figs. 3 and 4). The density is 0.1 e Å^{-3} at the O-atom site in $MnCO_3$ (Fig. 4). The ordering is not that of the cell volumes, with which the CO_3 group vibration amplitudes correlate, since magnesite has a smaller cell than calcite. The difference-map topography varies systematically with the mean electron density and with the correlated refractive indices.

* See deposition footnote.

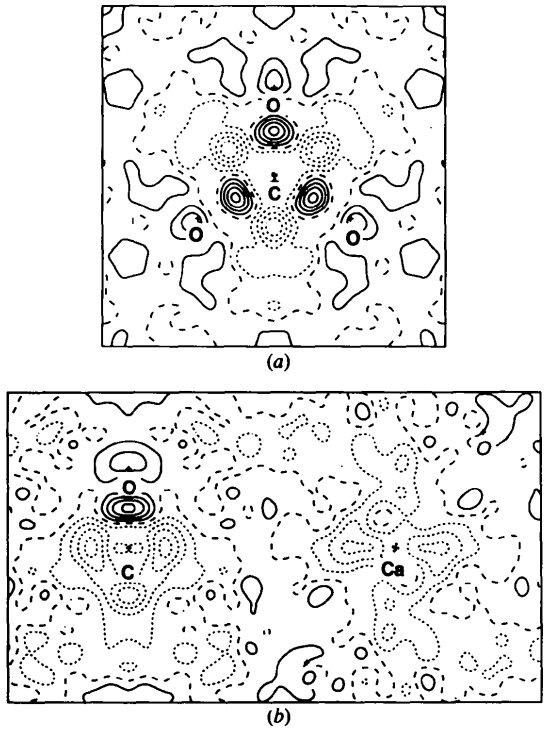

Fig. 2. $\Delta\rho$ for $CaCO_3$, evaluated with extinction corrections which minimize differences between equivalent reflection intensities. (*a*) (0001) plane through three O atoms of the CO_3 group; map borders 5.0 × 5.0 Å. (*b*) (01$\bar{1}$0) plane through Ca, C and O atoms with two O atoms deviating from the plane by ±0.33 Å shown in italics; map borders 8.5 × 5.0 Å. Contour interval 0.1 e Å^{-3}, positive, negative contours – solid, short dashes, respectively.

Maxima along the C—O bonds in the $\Delta\rho$ maps for $CaCO_3$ are lower and more localized than those in the maps in Figs. 3 and 4. The two-lobe shape of the charge distribution around the O atoms characteristic of lone pairs is less prominent and vibrationally smeared in calcite. The rhodochrosite $\Delta\rho$ maps have the most strongly anisotropic charge distribution, with broad clouds of the $\Delta\rho$ density surrounding the CO_3 group as displayed in Fig. 4(*b*). The withdrawal of electron density from the angular sectors between C—O vectors in the CO_3 group plane and the negative $\Delta\rho$ features in directions perpendicular to this plane contract and become progressively sharper from rhodochrosite through magnesite to calcite. Stronger depletion of CO_3 group density in $CaCO_3$ might be attributed to greater exchange depletion when the more diffuse radial electron distribution of the Ca cation overlaps with the CO_3 group.

The marked change in CO_3 group polarization from Figs. 2(*a*), 3(*a*) to 4(*a*) is consistent with the hypothesis that static polarization reflects what is expected from the refractive indices. Polarization is strongest for rhodochrosite, which has the highest refractive index. The strong antisymmetric component in the $\Delta\rho$ map maximizes in the (0001) basal plane through the CO_3 group, as expected because the refractive index maximizes for radiation with its electric vector aligned in

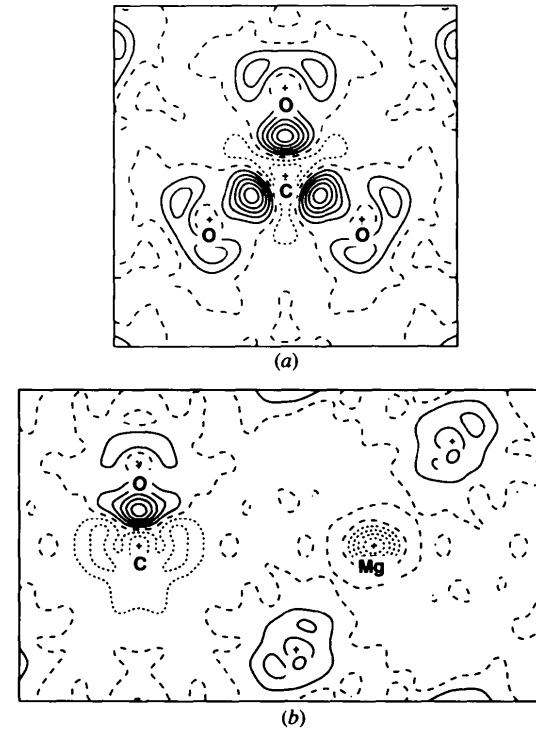

Fig. 3. $\Delta\rho$ for $MgCO_3$. (*a*) (0001) plane through three O atoms of the CO_3 group. (*b*) (01$\bar{1}$0) plane through Mg, C and O atoms with two O atoms deviating from the plane by ±0.22 Å shown in italics. Map borders and contours as for Fig. 2.

that plane. Locally antisymmetric components parallel to the c axis in the $\Delta\rho$ map are far less prominent, as expected from the relatively low n_e index.

For all CO_3 groups in these compounds the difference-density maxima at the middle of each C—O bond are elongated perpendicular to that bond in the manner expected for π-bonding between C and O atoms. The π-electron system for the CO_3 group is especially prominent for $MnCO_3$. The electron density elongates markedly along the c direction from C to the Mn atom. Coupling of spins *via* π-bonding in the CO_3 group could thus play a role in antiferromagnetic spin coupling for $MnCO_3$.

The aspherical charge distribution around the Mn atom in $MnCO_3$ can be related to splitting of the transition-metal 3*d*-orbital energies by the crystal field anisotropy that provides a basis for spin coupling. The distorted octahedral crystal field, quantized along the threefold axis, splits the fivefold-degenerate 3*d* state (Ballhausen, 1962) into a stable pair of σ-bonding e_g orbitals directed toward the nearest-neighbour O atoms, a pair of e_t orbitals directed approximately toward common octahedral site edges, and an a_t (d_{z^2}) orbital directed along the c axis toward the CO_3 group through an octahedral site face. The topography of the $MnCO_3$ $\Delta\rho$ maps suggests increased occupancy for the d_{z^2} orbital.

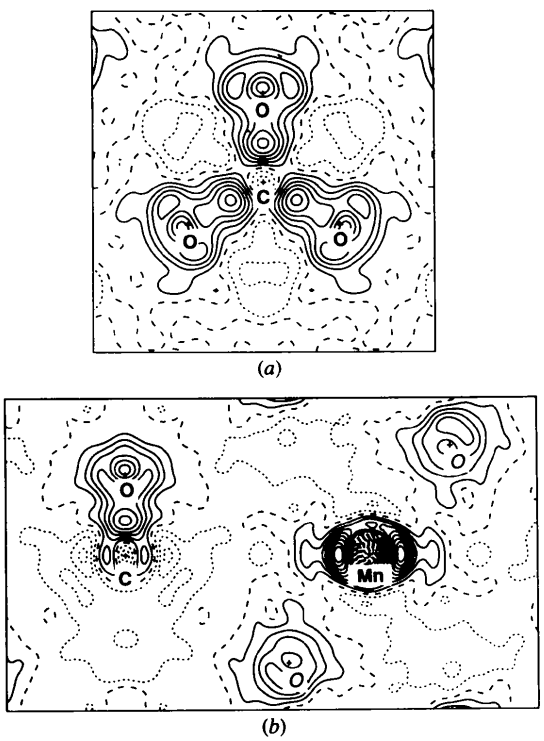

Fig. 4. $\Delta\rho$ for $MnCO_3$. (*a*) (0001) plane through three O atoms of the CO_3 group. (*b*) (01$\bar{1}$0) plane through Mn, C and O atoms with two O atoms deviating from the plane by ±0.26 Å shown in italics. Map borders and contours as for Fig. 2.

The relationship of the $\Delta\rho$ topography to the structural geometry suggests that the d_{z^2} orbital electrons for Mn interact with electrons in the C-atom p_z orbital. Direct interaction of the π-system of the CO_3 moiety with the metal atom is suggested as the degree of complexity in $\Delta\rho$ near the metal matches that near the CO_3 group spaced $c/4$ from the metal. Such an interaction along the c axis involves a 180° cation–anion–cation chain (Goodenough, 1963), generating $\Delta\rho$ features directed along a vector parallel to c linking the C and Mn nuclei. Covalency in the Mn—C interaction should be limited as the Mn—C distance along the c axis is 3.048 (2) Å. This argument is reinforced by the featureless $\Delta\rho$ topography near the centre of the Mn–CO_3 vector in the map in Fig. 4(*b*).

The ring of positive $\Delta\rho$ density around the Mn cation in Fig. 4(*b*) is consistent with expansion of the Mn^{2+} 3*d* radial wavefunction in the crystalline field compared with the free cation predicted by Freeman & Watson (1960) and confirmed by Hubbard, Rimmer & Hopgood (1966). There is approximate mirror (or twofold) $\Delta\rho$ density symmetry around the Mn cation in the plane of Fig. 4(*b*). A 6/*mmm* local symmetry in the $\Delta\rho$ map through the cations in the basal plane section (not reproduced here) is higher than the threefold symmetry of the cation–oxygen bond geometry. This higher density symmetry reflects the sixfold cation neighbour coordination in the basal plane. The cation influence is reduced for magnesite and completely subordinate to the anion geometry for calcite.

Discussion

The synchrotron $\Delta\rho$ densities for $CaCO_3$, $MgCO_3$ and $MnCO_3$ resemble those for $CaCO_3$ and $MgCO_3$ measured with Mo $K\alpha$ radiation (Maslen, Streltsov & Streltsova, 1993*a*,*b*) and are consistent with the hypothesis that the $\Delta\rho$ topography should reflect the variation in the refractive indices. The refractive index should be large when the locally antisymmetric components are strong and small for directions such that locally symmetric components in the density dominate.

Expression (1) shows why refractive index correlates strongly with the mean electron density $\bar{\rho}$ in the crystal. Deviations from simple proportionality for some carbonates listed in Table 1 show that $< n >^2 - 1$ may vary somewhat more than $\bar{\rho}$ due to the effect of the denominator K in (1). K measures the stiffness of the electrostatic interaction between mobile electrons and the nuclear framework (the electron–electron contribution to the electrostatic force vanishes) and is describable in terms of the second derivative of a potential energy. Differentiation occurs with respect to the displacement of the centre mass of the rigidly moved (polarized) electron density by the electric field. Expression (1) may be used provided only the more mobile rigidly moving electrons are included. The main contribution is expected to come

from regions where the potential is low and the electron density is relatively high. That holds for bonds, but must also apply to some extent to lone pairs.

Estimates of the 'procrystal' contribution to the crystal potential at the C—O bond in $CaCO_3$, $MgCO_3$ and $MnCO_3$ indicate that the potential, gradient and Laplacian of potential decrease progressively from calcite to rhodochrosite. Environmental effects of the cations on the CO_3 group, reflected in the progressive accumulation of $\Delta\rho$ density along the C—O bond in $CaCO_3$, $MgCO_3$ and $MnCO_3$, slowly increase K compared with the mean density $\bar{\rho}$ in (1). This could explain why these crystals' optical refractive indices increase in the series from calcite to rhodochrosite. Breakdown of the correlation between refractive indices and the $\bar{\rho}$ density for Cd, Co and Zn carbonates in Table 1 may reflect different behaviour for K and, consequently, $\Delta\rho$ density in these compounds. Electron-density studies of these carbonates could extend our understanding of their optical properties.

Superexchange interaction between 3*d* cations involving the CO_3 group, for which there is phenomenological evidence, can be accounted for by a correlation effect. Goodenough (1963) contends that the limited overlap near the mid-point of the interaction between the metal atom and the CO_3 group vector is inconsistent with the electron delocalization required for covalent bonding. This appears to be a convoluted way of asserting that the magnitude of the exchange term, originating in the antisymmetry of the electron wavefunction under the exchange of electrons between the interacting Mn and C atoms, is limited by the modest degree of overlap between them. The correlation mechanism is supposed to account for simultaneous partial bond formation (*i.e.* spin correlation) on each side of the CO_3 anion. The close topographical relationship between the $\Delta\rho$ maps near the metal atom and the C atom in Figs. 2(*b*), 3(*b*) and 4(*b*) suggests that interaction between these atoms does have a significant effect on the one-electron density. This view is consistent with the small magnitudes of two-electron correlation effects which in most cases are much less than the larger one-electron terms.

An alternative explanation for superexchange is that it originates in coupling of Mn—O—Mn interactions involving e_g orbitals of the Mn atom directed toward the nearest-neighbour O atoms, acting *via* the intermediary of the O anions coordinated octahedrally with both metals. Because of the structural geometry that would involve an intermediate-angle 119.82 (4)° Mn—O—Mn interaction. Although angle-dependent factors in the overlap integral between the Mn and its coordinated O-atoms' orbitals would be less than those in overlap between a C-atom p_z state and a Mn-atom d_{z^2} orbital, radial factors for the former would be larger than those for the latter, because of the smaller distances involved.

The high approximate symmetry of the accurate synchrotron $\Delta\rho$ density in $MnCO_3$ suggests that 3*d* metal cations deform the electron density more strongly than the O atoms and lighter cations. Overlapping atomic electron densities are deformed mainly by interactions involving the cations in the basal plane. Electron density overlapping with the closed inner subshells of the heavy 3*d* cations is transferred by exchange to regions of lower electrostatic potential further from the nuclei retaining the cations' symmetry. These long distance cation–cation interactions can be associated with weak ferromagnetic ordering in the basal plane of the $MnCO_3$ structure. Pronounced accumulation and anisotropy of the $\Delta\rho$ charge density near the CO_3 group in $MnCO_3$ determined from the accurate synchrotron data, supposedly responsible for the higher optical anisotropy of $MnCO_3$, correlates with delocalization and developing spin density observed near this group by Brown & Forsyth (1967). In the magnetic case marked coupling is expected to be dominated by locally symmetric components in the density, because magnetic dipole interactions are described by axial vectors, whereas electric interactions, for which antisymmetric density components are more important, are described by polar vectors.

This work was supported by the Australian Research Council. Financial support by the Australian National Beamline Facility (ANBF) is also acknowledged. The ANBF is funded by a consortium comprising the ARC, DITARD, ANSTO, CSIRO, ANU and UNSW. We are indebted to Professor D. C. Creagh for assistance in calculating absorption and dispersion corrections and to Mr A. B. Fletcher (CSIRO) for assistance in growing magnesite crystals by the hydrothermal method.

References

ALCOCK, N. W. (1974). *Acta Cryst.* A**30**, 332–335.
BALLHAUSEN, C. (1962). *Introduction to Ligand Field Theory*. New York: McGraw-Hill.
BORODIN, V. L., LYUTIN, V. I., ILYUKHIN, V. V. & BELOV, N. V. (1979). *Sov. Phys. Dokl.* **24**, 226–227.
BRAGG, W. L. (1924). *Proc. R. Soc. London Ser. A*, **105**, 370–386.
BROWN, P. J. & FORSYTH, J. B. (1967). *Proc. Phys. Soc.* **92**, 125–135.
CATTI, M., PAVESE, A., APRA, E. & ROETTI, C. (1993). *Phys. Chem. Min.* **20**, 104–110.
CATTI, M., PAVESE, A., DOVESI, R. & SAUNDERS, V. R. (1993). *Phys. Rev. B*, **47**, 9189–9198.
CREAGH, D. C. (1992). Private communication.
CRUICKSHANK, D. W. J. (1949). *Acta Cryst.* **2**, 65–82.
DZIALOSHINSKII, E. I. (1957). *Sov. Phys. JETP*, **5**, 1259–1271.
EFFENBERGER, H., MEREITER, K. & ZEMANN, J. (1981). *Z. Kristallogr.* **156**, 233–243.
FINGER, L. W. (1975). *Carnegie Inst. Washington Yearb.* **74**, 572–575.
FREEMAN, A. J. & WATSON, R. E. (1960). *Phys. Rev.* **118**, 1168–1172.
GOODENOUGH, J. B. (1963). *Magnetism and the Chemical Bond*. New York, London: Interscience Publishers.
GRAF, D. L. (1961). *Am. Mineral.* **46**, 1283–1316.
HALL, S. R., FLACK, H. D. & STEWART, J. M. (1992). *Xtal3.2 Reference Manual*. Univs. of Western Australia, Australia, and Maryland, USA.
HANSON, W. F., ARAKAWA, E. T. & WILLIAMS, M. W. (1972). *J. Appl. Phys.* **43**, 1661–1665.
HELLWEGE, K. H., LESCH, W., PLIHAL, M. & SCHAACK, G. (1970). *Z. Physik.* **232**, 61–86.

HIRSHFELD, F. L. (1977). *Isr. J. Chem.* **16**, 198–201.
HUBBARD, J., RIMMER, D. E. & HOPGOOD, F. R. A. (1966). *Proc. Phys. Soc.* **88**, 13–36.
ISHERWOOD, B. J. & JAMES, J. A. (1976). *Acta Cryst.* A**32**, 340–341.
KITTEL, C. (1986). *Introduction to Solid State Physics*, 6th ed. New York: John Wiley & Sons.
LARSON, A. C. (1970). *Crystallographic Computing*, edited by F. R. AHMED, pp. 291–294. Copenhagen: Munksgaard.
LINDGÅRD, P. A. & MARSHALL, W. (1969). *J. Phys. C*, **2**, 276–287.
MAMEDOV, A. M., SHILNIKOV, V. I., MEHDIEV, T. R. & IBRAGIMOVA, I. S. (1984). *Physica (Utrecht) B*, **123**, 156–168.
MASLEN, E. N. & SPADACCINI, N. (1993). *Acta Cryst.* A**49**, 661–667.
MASLEN, E. N., STRELTSOV, V. A. & STRELTSOVA, N. R. (1993*a*). *Acta Cryst.* B**49**, 636–641.
MASLEN, E. N., STRELTSOV, V. A. & STRELTSOVA, N. R. (1993*b*). *Acta Cryst.* B**49**, 980–984.
MASLEN, E. N., STRELTSOV, V. A., STRELTSOVA, N. R. & ISHIZAWA, N. (1994). *Acta Cryst.* B**50**, 435–441.
MASLEN, E. N., STRELTSOV, V. A., STRELTSOVA, N. R., ISHIZAWA, N. & SATOW, Y. (1993). *Acta Cryst.* B**49**, 973–980.
MORANDAT, J., LORENZELLI, V. & LECOMTE, J. (1967). *J. Phys.* **28**, 152–156.
NATHANS, R., PICKART, S. J., ALPERIN, H. A. & BROWN, P. J. (1964). *Phys. Rev. A*, **136**, 1641–1647.
OH, K. D., MORIKAWA, H., IWAI, S. & AOKI, H. (1973). *Am. Mineral.* **58**, 339–340.
PRINCE, E., SCHROEDER, L. W. & RUSH, J. J. (1973). *Acta Cryst.* B**29**, 184–191.
REEDER, R. J. (1983). Editor. *Carbonates: Mineralogy and Chemistry, Reviews in Mineralogy*, Vol. 11, pp. 1–47. Chelsea, Michigan: BookCrafters.
REES, B. (1977). *Isr. J. Chem.* **16**, 180–186.
SATOW, Y. & IITAKA, Y. (1989). *Rev. Sci. Instrum.* **60**, 2390–2393.
SCHOMAKER, V. & TRUEBLOOD, K. N. (1968). *Acta Cryst.* B**24**, 63–76.
STRELTSOV, V. A. & ZAVODNIK, V. E. (1989). *Sov. Phys. Cryst.* **34**(6), 824–828.
TOSSEL, J. A. & LAZZERETTI, P. (1988). *Phys. Rev. B*, **38**, 5694–5698.
WEBER, H.-J. (1988). *Acta Cryst.* A**44**, 320–326.
WHITE, W. B. (1974). *The Infrared Spectra of Minerals*, edited by V. C. FARMER, pp. 227–284. London: Mineralogical Society.
ZACHARIASEN, W. H. (1967). *Acta Cryst.* A**23**, 558–564.

Acta Cryst. (1995). B**51**, 939–942

A Synchrotron Radiation Study of Strontium Titanate

BY E. N. MASLEN AND N. SPADACCINI

Crystallography Centre, University of Western Australia, Nedlands 6009, *Western Australia*

T. ITO

Department of Chemical Technology, Kanagawa Institute of Technology, Atsugi, Kanagawa 243-02, *Japan*

F. MARUMO

Research Laboratory of Engineering Materials, Tokyo Institute of Technology, Nagatsuta-machi 4259 *Midori-ku, Yokohama* 227, *Japan*

AND Y. SATOW

Faculty of Pharmaceutical Sciences, University of Tokyo, 7-3-1 *Hongo Bunkyo-ku, Tokyo* 113, *Japan*

(*Received* 8 *February* 1994; *accepted* 7 *March* 1995)

Abstract

Electron deformation densities $\Delta\rho$ for $SrTiO_3$ have been determined from diffraction data measured using focused synchrotron radiation with $\lambda = 0.7000(2)$ Å at the Photon Factory, KEK, Japan. Corrections for secondary extinction were estimated from the variation of diffraction intensity with path length, and checked from the λ-dependence of the strong intensities indicated by measurements using a weaker parallel beam with $\lambda = 0.5000(2)$ Å. The 0.7 Å study is more precise than earlier analyses with Mo $K\alpha$ radiation. The difference density near the Ti nucleus is mildly anisotropic, and the $\Delta\rho$ topography is similar to those for closed-shell atoms in related perovskite structures.

Introduction

At room temperature $SrTiO_3$ is isomorphous with the KMF_3 compounds with M = Mn, Co, Fe, Ni and Zn, which have the cubic $Pm\bar{3}m$ structure that characterizes the perovskite series. There is strong scientific interest in this series, partly because of the ferroelectricity, superconductivity and other technologically important properties of particular members. Some of these properties are related to deviations from the ideal structure. Full understanding of the effect of structural distortions is more likely to be achieved when the ideal case is thoroughly understood.

Diffraction studies of $SrTiO_3$ with Mo $K\alpha$ radiation by Buttner & Maslen (1992) yielded atomic charges

ISSN 0108-7681